A local equilibrium model for tokamak plasmas: theory and applications.

P. Rodrigues[1], F. Cella[2,1], and A. Coroado[3,1]

[1]*Instituto de Plasmas e Fusão Nuclear, Instituto Superior Técnico, Universidade de Lisboa, 1049-001 Lisboa, Portugal.*

[2]*Dipartimento di Energia, Politecnico di Milano, Via Ponzio 34/3, 20133 Milan, Italy.*

[3]*École Polytechnique Fédérale de Lausanne (EPFL), Swiss Plasma Center (SPC), CH-1015 Lausanne, Switzerland.*

Local equilibrium model.

Magnetic equilibria are fundamental to most phenomena in tokamak plasmas, but accurate numerical solutions of the Grad-Shafranov (GS) equation

$$-R\nabla\cdot\left(R^{-1}\nabla\Psi\right)=\mu_0R^2p'+FF'=-\mu_0J_\phi(R,\Psi), \tag{1}$$

where Ψ is the poloidal flux per radian such that $\mathbf{B}=\nabla\phi\times\nabla\Psi+B_\phi\nabla\phi$, are not always the best tool to gain analytical insight into such complex processes. Simplified local descriptions, like the $s-\alpha$ model with circular magnetic surfaces [2] are not able to capture plasma-shaping effects. More elaborate models, like the Miller one [3], involve non-orthogonal coordinates and non-trivial metric tensors, which results in intricate expressions for the magnetic-field components. Therefore, they are unsuitable for analytically driven work on plasma-shaping effects.

A new approach intended to provide analytically tractable field components has been presented recently [1], which focus on a simple analytical description of the poloidal flux instead of a detailed or intuitive description of the magnetic-surface shape. Using the poloidal cross section coordinates $\{x=R/R_0,\,y=Z/R_0\}$, the flux normalised to its boundary value ($\psi=\Psi/\Psi_\mathrm{b}$) can be written as a Solovev solution [4]

$$\psi=\underbrace{-\tfrac{1}{8}S_\mathrm{p}x^4-\tfrac{1}{2}S_\mathrm{F}x^2\ln x}_{\text{particular solution}}+\underbrace{\hat{c}_0+\sum_{i=1}^{4}\overbrace{\hat{c}_i\hat{\psi}_\mathrm{h}^i}^{\text{sym}}+\overbrace{\check{c}_i\check{\psi}_\mathrm{h}^i}^{\text{asym}}}_{\text{homogeneous solution}}, \tag{2}$$

where the local coefficients $S_\mathrm{p},S_\mathrm{F},\hat{c}_i,\check{c}_i$ are assumed constant along flux surfaces, but allowed to change slowly across them. Around each magnetic surface, the local approximation is valid within a region $\Delta\psi$ such that $\left|\Delta\psi J_\phi^{-1}\,\partial_\psi J_\phi\right|\ll 1$. Up-down symmetric and asymmetric homogeneous solutions [4] enable a suitable description of the plasma shape. After changing to the orthogonal coordinates $\{r=\varepsilon^{-1}\sqrt{(x-1)^2+y^2},\,\theta=\mathrm{atan}(y/x)\}$, where $\varepsilon=a/R_0$ is the inverse aspect ratio, the normalised flux becomes

$$\psi(r,\theta)=S_0r^2\left[\Theta_0(\theta)+\varepsilon r\Theta_1(\theta)+\varepsilon^2r^2\Theta_2(\theta)+\cdots\right], \tag{3}$$

with the angular functions $\Theta_i(\theta)$ being defined as

$$\begin{aligned}&\Theta_0(\theta)=1+\hat{\kappa}\cos2\theta+\check{\kappa}\sin2\theta,\quad \Theta_1(\theta)=\hat{\Delta}\cos\theta+\tfrac{1}{4}\check{\kappa}\sin\theta+\hat{\eta}\cos3\theta+\check{\eta}\sin3\theta,\\ &\Theta_2(\theta)=\frac{8\hat{\Delta}-3\hat{\kappa}-3}{32}+\frac{2\hat{\eta}+2\hat{\Delta}-\hat{\kappa}-1}{8}\cos2\theta+\frac{4\check{\eta}-\check{\kappa}}{16}\sin2\theta+\hat{\chi}\cos4\theta+\check{\chi}\sin4\theta.\end{aligned} \tag{4}$$

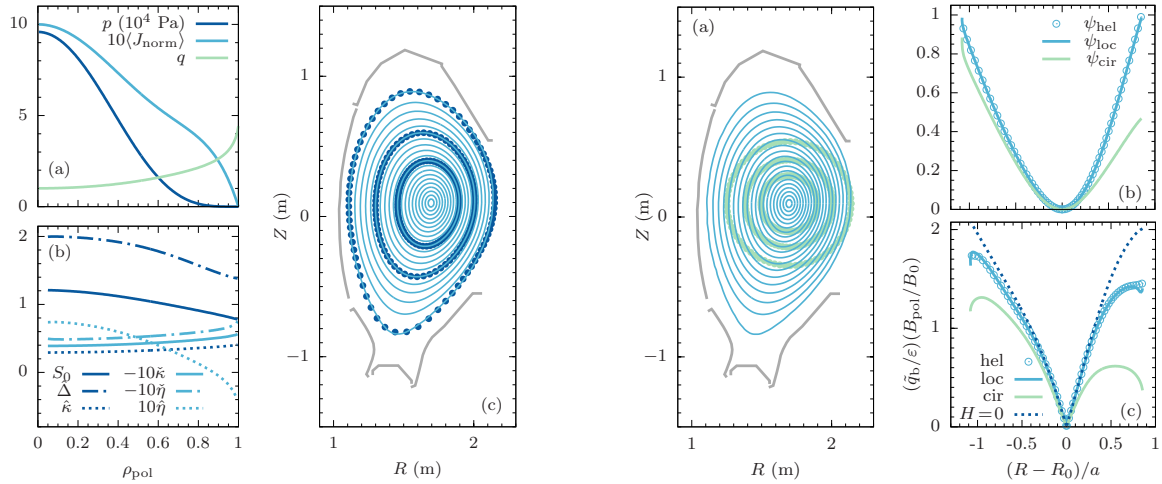

Figure 1: Left panel — Pressure, toroidal current density, and safety factor (a); fitted coefficients (b); numerical magnetic surfaces [(c), lines] and analytical ones [(c), large dots]. Right panel — HELENA equilibrium [(a), lines] and circular model [(a), large dots]; ψ (b) and poloidal field (c) on the midplane (HELENA, local, and circular models).

Equation (3) can be inverted for a given flux value, yielding the flux-surface parametrisation

$$r(\theta) = \tilde{s}\left(\frac{1}{\Theta_0^{1/2}} - \frac{\Theta_1}{2\Theta_0^2}\tilde{\varepsilon} + \frac{5\Theta_1^2 - 4\Theta_0\Theta_2}{8\Theta_0^{7/2}}\tilde{\varepsilon}^2 + \cdots\right), \tag{5}$$

where $\tilde{s} = \sqrt{\psi/S_0}$ and $\tilde{\varepsilon} \equiv \varepsilon\tilde{s}$. In turn, the conventional definitions ρ, Δ, and κ [3] are recovered:

$$\frac{\rho}{a} \approx \frac{\tilde{s}}{\sqrt{1+\hat{\kappa}}}, \quad \kappa \approx \sqrt{\frac{1+\hat{\kappa}}{1-\hat{\kappa}}}, \quad \frac{\Delta}{a} \approx -\frac{\varepsilon\tilde{s}^2}{2}\frac{\hat{\Delta}+\hat{\eta}}{\left(1+\hat{\kappa}\right)^2}. \tag{6}$$

The magnetic-field components are written as

$$B^r(r,\theta) = -r\frac{B_0}{R}\frac{S_0}{\tilde{q}_\mathrm{b}}\frac{\dot{\Theta}_0 + \varepsilon r\dot{\Theta}_1 + \varepsilon^2 r^2\dot{\Theta}_2}{1-H}, \quad B^\theta(r,\theta) = \frac{B_0}{R}\frac{S_0}{\tilde{q}_\mathrm{b}}\frac{2\Theta_0 + 3\varepsilon r\Theta_1 + 4\varepsilon^2 r^2\Theta_2}{1-H},$$
$$B_\phi(r,\theta) = B_0 R_0\sqrt{1+\varepsilon^2 S_\mathrm{d}\psi(r,\theta)}, \tag{7}$$

with $H = r^2\left[\left(S_0\Theta_0\right)' + \varepsilon r\left(S_0\Theta_1\right)' + \varepsilon^2 r^2\left(S_0\Theta_2\right)'\right]$ the implicit radial dependence, $\tilde{q}_\mathrm{b} = B_0 a^2/\Psi_\mathrm{b}$, and S_d a new local coefficient. The ability of the local model to describe realistic tokamak plasmas is tested with a numerical equilibrium computed by HELENA [7] for typical ASDEX-Upgrade parameters [1]. The results are plotted in figure 1.

Application 1: Straight-field coordinates and finite magnetic shear.

The coordinates $\{\psi, \chi, \phi\}$, where the poloidal angle $\chi(r,\theta)$ is defined such that

$$b^\phi = q(\psi)b^\chi = q(\psi)\left(b^r\partial_r\chi + b^\theta\partial_\theta\chi\right), \tag{8}$$

with $\mathbf{b} = \mathbf{B}/B$ the magnetic field-line versor, are a key element in MHD stability codes. For shaped plasmas, $q(\psi)$ must be expanded around a surface labelled by ψ_i as

$$q(\psi) = q_i + q_i'\left(\psi - \psi_i\right) + \cdots = \frac{\tilde{q}_\mathrm{b}}{2S_0}\left(\frac{1}{\tilde{\iota}} + \xi\tilde{s}^2 + \cdots\right), \; \xi = 2S_0\frac{q_i'}{q_i}, \; \frac{1}{\tilde{\iota}} = 2S_0\frac{q_i}{\tilde{q}_\mathrm{b}}\left(1 - \psi_i\frac{q_i'}{q_i}\right). \tag{9}$$

The solution of equation (8) can thus be sought as a series in the small parameters ε, ξ, yielding

$$\begin{aligned}\chi(r,\theta) &= \chi_0(\theta)\Big(1-\xi r^2\tilde{\iota}\Theta_0\Big) - \varepsilon r\frac{\tilde{\iota}(1-\hat{\kappa})^2}{\tilde{\kappa}^4\Theta_0}\sin\theta + \cdots,\\ \chi_0(\theta) &= \frac{\tilde{\iota}}{\tilde{\kappa}}\Big[\arctan\frac{\check{\kappa}+(1-\hat{\kappa})\tan\theta}{\tilde{\kappa}} - \arctan\frac{\check{\kappa}}{\tilde{\kappa}}\Big], \quad \text{with} \quad \tilde{\kappa}+\hat{\kappa}+\check{\kappa}=1.\end{aligned} \tag{10}$$

Discarding the shaping, the solution simplifies to $\chi(r,\theta) = \tilde{\iota}\big(1-\tilde{\iota}\xi r^2\big)\theta - \tilde{\iota}\varepsilon r\sin\theta + \cdots$, which can be further reduced to previous results [9] in the no-shear limit ($\xi = 0, \tilde{\iota} = 1$).

Application 2:Guiding-centre analytical orbits.

Besides energy and magnetic moment E, μ (and thus $\Lambda = \mu B_0/E$), the momentum

$$\frac{P_\phi}{-q_\mathrm{s}\Psi_\mathrm{b}} \equiv \tilde{P}_\phi = \psi(r,\theta) - \frac{m_\mathrm{s}}{q_\mathrm{s}\Psi_\mathrm{b}} v_\parallel \frac{B_\phi(r,\theta)}{B(r,\theta)} \tag{11}$$

is also a constant of motion in guiding-centre theory. Replacing $\psi(r,\theta)$, $B_\phi(r,\theta)$, and $B(r,\theta)$ by their corresponding series, a solution can be sought as a series $r_\mathrm{orb}(\theta) = r_0(\theta) + \varepsilon r_1(\theta) + \cdots$ by recursively solving for each coefficient $r_i(\theta)$. Defining $[r_\mathrm{orb}(0) - r_\mathrm{orb}(\pi)]/2 \equiv \Delta_\mathrm{orb}$ and noticing that $[r_\mathrm{orb}(0) + r_\mathrm{orb}(\pi)]/2 = \tilde{s} + \cdots$, the orbit for passing particles ($\tilde{\Lambda}_\mathrm{p} \equiv 1 - \Lambda \sim 1$) is written as

$$\frac{r_\mathrm{orb}(\theta)}{\tilde{s}} = \underbrace{\frac{1}{\Theta_0^{1/2}} - \tilde{\varepsilon}\,\frac{\Theta_1}{2\Theta_0^2}}_{\text{guiding terms}} + \underbrace{\tilde{\delta}_\mathrm{p}\frac{\cos\theta}{\Theta_0}}_{\text{drift term}} + \cdots, \quad \tilde{\delta}_\mathrm{p} \equiv \frac{\Delta_\mathrm{orb}}{\tilde{s}}, \quad \tilde{s}^2 \equiv \frac{\tilde{P}_\phi}{S_0} + \frac{4\Delta_\mathrm{orb}\tilde{\Lambda}_\mathrm{p}}{\varepsilon\big(1+\tilde{\Lambda}_\mathrm{p}\big)}. \tag{12}$$

The lowest-order transit frequency is $v_\parallel/(\tilde{q}R_0)$ [8] and shaping effects change it to

$$\omega_\mathrm{t} = \frac{v_\parallel}{\tilde{q}R_0}\frac{\sqrt{1-(\hat{\kappa}^2+\check{\kappa}^2)}}{1-\hat{\kappa}} + \mathscr{O}(\varepsilon^2, \tilde{\delta}_\mathrm{p}^2). \tag{13}$$

In turn, the orbit for trapped particles [$\tilde{\Lambda}_\mathrm{t} \equiv (1-\Lambda)/\tilde{\varepsilon} \sim 1$] is written as

$$\frac{r_\mathrm{orb}(\theta)}{\tilde{s}} = \underbrace{\frac{1}{\Theta_0^{1/2}} - \frac{\tilde{\varepsilon}\Theta_1}{2\Theta_0^2}}_{\text{guiding terms}} \underbrace{- \frac{\tilde{\delta}_\mathrm{t}\tilde{\Lambda}_\mathrm{t}}{2\Theta_0^{1/2}} + \tilde{\delta}_\mathrm{t}^{1/2}\sqrt{\frac{\cos\theta + \tilde{\Lambda}_\mathrm{t}\Theta_0^{1/2}}{\Theta_0^{3/2}}} + \cdots}_{\text{drift terms}}, \quad \tilde{s}^2 \equiv \frac{\tilde{P}_\phi}{S_0}, \quad \tilde{\delta}_\mathrm{t}^{1/2} \equiv \frac{\Delta_\mathrm{orb}}{\tilde{s}\sqrt{1+\tilde{\Lambda}_\mathrm{t}}}, \tag{14}$$

and the shaping effect on the orbit's tip is $\cos\theta_\mathrm{tip} = -\tilde{\Lambda}_\mathrm{t}\Big[1 - \big(\tfrac{1}{2} - \tilde{\Lambda}_\mathrm{t}^2\big)\hat{\kappa} - \tilde{\Lambda}_\mathrm{t}\sqrt{1-\tilde{\Lambda}_\mathrm{t}^2}\check{\kappa} + \cdots\Big]$.

Application 3: Geodesic curvature and MHD shear/acoustic continua coupling.

MHD perturbations $\xi \propto e^{i(\omega t + m\theta + n\phi)}$ split in shear ($\eta = \xi \cdot \frac{\mathbf{B}\times\nabla\Psi}{|\nabla\psi|^2}$) and sonic ($\zeta = \nabla\cdot\xi$) components that become singular at the pairs $\{\psi, \omega\}$ (the MHD continua) for which

$$\begin{bmatrix} \frac{\omega^2}{v_\mathrm{A}^2}|\nabla\Psi|^2 + B_0\nabla_\parallel\big(|\nabla\Psi|^2\frac{\nabla_\parallel}{B_0}\big) & \frac{v_\mathrm{S}^2}{v_\mathrm{A}^2}B_0^2K_s \\ K_s & 1 + \frac{v_\mathrm{S}^2}{v_\mathrm{A}^2} + \frac{v_\mathrm{S}^2}{\omega^2}B_0\nabla_\parallel\big(\frac{\nabla_\parallel}{B_0}\big) \end{bmatrix} \begin{bmatrix}\eta \\ \zeta\end{bmatrix} = 0, \tag{15}$$

where $\kappa = (\mathbf{b}\cdot\nabla)\mathbf{b}$ and $K_s = 2B^{-2}(\kappa\times\mathbf{B})\cdot\nabla\Psi$, while v_A and v_S are the Alfvén and sonic velocities [5]. The two continua branches are coupled by a non-vanishing geodesic curvature K_s, whose harmonics produce frequency gaps proportional to their amplitude and to $v_\mathrm{A}^2/v_\mathrm{S}^2 \sim \beta$.

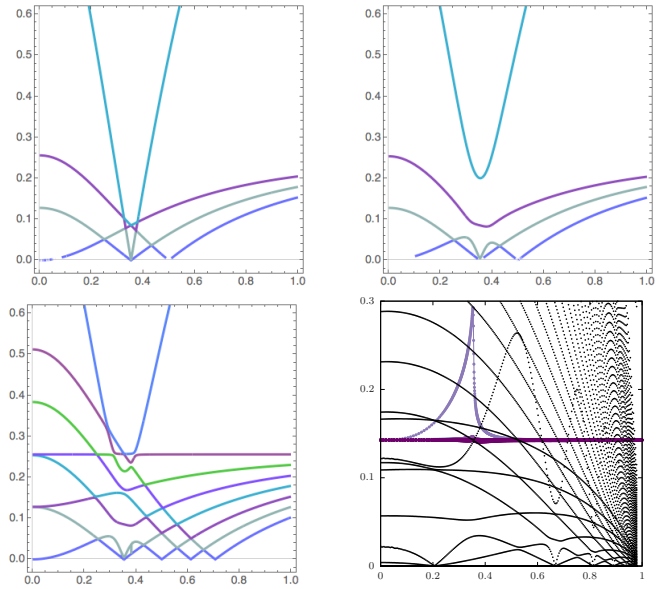

Figure 2: Decoupled shear-Alfvén branch ($m = m_A$) and three sonic waves near a rational surface $nq = m$ (a); Four-mode coupling by a single harmonic in K_s (b); Eight-mode coupling by additional harmonics (c); Numerical continua and gap eigenmode (d).

For a circular equilibrium, $K_s = \tilde{\varepsilon} q^{-1} \sin\theta$ and a four-wave coupling opens a low-frequency gap [6]. On the other hand, finite plasma shaping yields

$$K_s = \frac{\tilde{\varepsilon}}{q}\left[\left(1 - \tfrac{3}{4}\hat{\kappa}\right)\sin\theta - \tfrac{1}{4}\hat{\kappa}\sin 3\theta + \tfrac{3}{4}\check{\kappa}\cos\theta + \tfrac{1}{4}\check{\kappa}\cos 3\theta + \cdots\right] \tag{16}$$

and additional gaps arise in the continua, at about half the TAE frequency, where discrete eigenmodes can be found (figure 2).

In summary, a local equilibrium model was presented that is able to describe a realistic tokamak geometry and, simultaneously, able to allow tractable analytical work in a variety of contexts. Such analytical ability was illustrated with three particular examples.

Acknowledgments

IPFN activities were financially supported by "Fundação para a Ciência e Tecnologia" (FCT) via project UID/FIS/50010/2013. F. Cella was supported by FuseNet from the Euratom research and training programme under grant agreement no. 633053.

References

[1] P. Rodrigues and A. Coroado, Nucl. Fusion **58**. 106040 (2018).
[2] J. Connor *et al.*, Phys. Rev. Lett., **40**, 396 (1978).
[3] R. Miller *et al.*, Phys. Plasmas **5**, 973 (1998).
[4] A. Cerfon and J. Freidberg, Phys. Plasmas **17**, 032502 (2010).
[5] C. Cheng and M. Chance, Phys. Fluids **29**, 3695 (1986).
[6] B. van der Holst *et al.*, Phys. Plasmas **16**, 032308 (2000).
[7] G. Huysmans *et al.*, Int. J. Mod. Phys. C **2**, 371 (1991).
[8] H. Wong *et al.*, Nucl. Fusin **35**, 1721 (1995).
[9] X. Lapillonne *et al.*, Phys. Plasmas **16**, 032308 (2009).